Geochemical Perspectives Letters

Planetary accretion and core formation inferred from Ni isotopes in enstatite meteorites

K. Zhu[1,2*], H. Becker[1], J.-M. Zhu[3*], H.-P. Xu[3], Q.-R. Man[3]

OPEN ACCESS

https://doi.org/10.7185/geochemlet.2306

Abstract

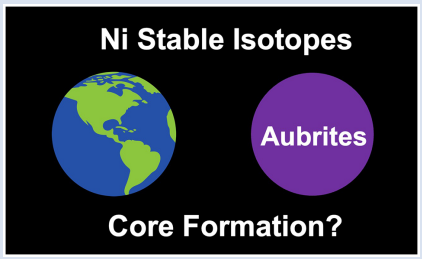

Nickel is a siderophile and near-refractory element, making its isotopes a potential tool for tracing planetary accretion and differentiation. However, the origin of the Ni stable isotope difference between bulk silicate Earth (BSE) and chondrites remains enigmatic. To address this problem, we report high precision Ni stable isotope data of enstatite chondrites and achondrites that possess similar mass independent O and Ni isotope compositions like the Earth-Moon system. Bulk enstatite chondrites have $\delta^{60/58}$Ni values of 0.24 ± 0.08 ‰ (2 s.d., $n = 13$). Enstatite achondrites, including main-group aubrites, Shallowater and Itqiy, show relatively large $\delta^{60/58}$Ni variations, ranging from 0.03 ± 0.02 ‰ to 0.57 ± 0.04 ‰. This could reflect fractionations between sulfide and metal phases, as is evidenced by correlation between their S/Ni ratios and $\delta^{60/58}$Ni values. In enstatite achondrites, Ni is mainly hosted in metal and to a lesser extent in sulfides, so $\delta^{60/58}$Ni values in enstatite achondrites may represent the Ni isotopic values of the cores of their parent bodies. The overlapping $\delta^{60/58}$Ni values between bulk enstatite achondrites and enstatite chondrites indicate limited Ni stable isotope fractionation during core formation processes on reduced, sulfur-rich parent bodies. The Ni stable isotope gap between chondrites and the BSE could be possibly explained by chondrule-rich accretion model.

Received 6 September 2022 | Accepted 31 January 2023 | Published 23 February 2023

Introduction

Core formation is one of the first planetary differentiation processes that can be reconstructed by using the stable isotope composition of siderophile elements. Nickel (Ni) is one such siderophile element; it is also a major element (>1 wt. %) in chondrites, nearly refractory ($T_{c50\ \%}$ of 1363 K), and occurs as Ni^0 and Ni^{2+} in planetary materials (Wood *et al.*, 2019). These properties suggest that Ni stable isotopes probably were not, or only little, fractionated by volatilisation and silicate differentiation processes (Klaver *et al.*, 2020; Wang *et al.*, 2021; Zhu *et al.*, 2022). Core formations in the Earth and other differentiated planets/asteroids can be traced by comparing the bulk Ni stable isotope compositions (represented by chondritic Ni isotope compositions) and Ni isotope compositions in the silicate portion.

Previous studies have investigated the Ni stable isotope composition (expressed as $\delta^{60/58}$Ni, the mass dependent deviation of $^{60}Ni/^{58}Ni$ ratios of samples relative to the ratio of NIST SRM 986, given in per mille) of chondrites with an average $\delta^{60/58}$Ni value of 0.23 ± 0.14 ‰ (2 s.d.) and of the bulk silicate Earth (BSE) with an average $\delta^{60/58}$Ni value of 0.10 ± 0.07 ‰ (2 s.d.) (Cameron *et al.*, 2009; Gall *et al.*, 2017; Klaver *et al.*, 2020; Wang *et al.*, 2021; Zhu *et al.*, 2022). Klaver *et al.* (2020) were the first to resolve a difference of Ni stable isotope compositions between the chondrites and BSE ($\Delta^{60/58}Ni_{Chondrites\text{-}BSE} \approx 0.13$ ‰), which is, however, impossible to explain by single stage terrestrial core formation. Evidences include 1) Ni isotope similarity between chondrites and mantle of ureilite parent body (Zhu *et al.*, 2022), 2) *ab initio* calculations (Guignard *et al.*, 2020; Wang *et al.*, 2021), and 3) high pressure experiments (Lazar *et al.*, 2012; Guignard *et al.*, 2020) which show that metal-silicate partitioning of Ni during core segregation at high temperatures and pressures would not induce measurable Ni stable isotope fractionation in Earth's mantle. Two scenarios were considered for this issue: 1) chondrites cannot represent bulk Earth while chondrules are potential precursor material of Earth (Zhu *et al.*, 2022), and 2) Wang *et al.* (2021) proposed a different model in which the object (Theia) that hit the Earth during the Moon-forming impact was Mercury-like, *i.e.* highly reduced, and its mantle may have been rich in sulfide with isotopically light Ni. According to this hypothesis, the impactor mantle merged into the Proto-Earth's mantle and decreased the chondritic $\delta^{60/58}$Ni value of the proto-Earth's mantle to the modern BSE value.

Enstatite achondrites, which include aubrites (most of them are brecciated; Table 1; Keil, 2010), come from the silicate portions of multiple differentiated asteroids that have similar isotope compositions as the Earth-Moon system (Clayton *et al.*, 1984; Zhu *et al.*, 2021). Depletion in highly siderophile elements (HSEs), supports the idea that their parent body (or bodies) have a core (van Acken *et al.*, 2012a). Therefore, comparing the Ni isotope signatures between enstatite achondrites and enstatite

1. Freie Universität Berlin, Institut für Geologische Wissenschaften, Malteserstr. 74-100, 12249 Berlin, Germany
2. Bristol Isotope Group, School of Earth Sciences, University of Bristol, Wills Memorial Building, Queen's Road, Bristol BS8 1RJ, United Kingdom
3. State Key Laboratory of Geological Processes and Mineral Resources, China University of Geosciences (Beijing), Beijing 100083, China
* Corresponding author (emails: K. Zhu, ke.zhu@bristol.ac.uk; J.-M. Zhu, jmzhu@cugb.edu.cn)

Table 1 Ni stable isotopic compositions of enstatite meteorites.

Meteorite	Fall/ Find	Type	Petrology	Mass (mg)	Mg#	S content (%)	Uncertainty	Ni content (ppm)	S/Ni	$\delta^{60/58}$Ni (‰)	2 s.d.	2 s.e.	*n*	References, notes
Enstatite chondrites														
GRO 95517	Find	EH3		7.8		4.0	0.2			**0.28**	0.03	0.02	2	
QingZhen	Fall	EH3		5.5		4.1	–			**0.27**	0.04	0.03	2	
SAH 97096	Find	EH3		33.2		4.4	0.5			**0.26**	0.06	0.04	2	
Kota-Kota	Find	EH3								**0.20**	0.03	0.01	8	Klaver *et al.* (2020)
Kota-Kota	Find	EH3								**0.26**	0.04			Wang *et al.* (2021)
Kota-Kota	Find	EH3								**0.21**	0.04			Wang *et al.* (2021)
Kota-Kota Avg.						3.6	0.1			**0.22**	0.06			
Indarch	Fall	EH4								**0.29**	0.05	0.04	2	
Indarch	Fall	EH4								**0.27**	0.09	0.03	9	Gall *et al.* (2017)
Indarch	Fall	EH4								**0.19**	0.03	0.01	8	Klaver *et al.* (2020)
Indarch Avg.						3.6	0.8			**0.22**	0.09			
Abee	Fall	EH4								**0.19**	0.05			Cameron *et al.* (2009)
Abee	Fall	EH4								**0.25**	0.02	0.01	5	Klaver *et al.* (2020)
Abee Avg.						4.5	0.9			**0.22**	0.09			
St. Mark's	Fall	EH5				3.3	0.9			**0.18**	0.02	0.01	15	Klaver *et al.* (2020)
MAC 88184	Find	EL3		4.6		2.2	0.1			**0.21**	0.08	0.05	2	
MAC 02837	Find	EL3		6.5		2.8	0.2			**0.35**	0.03	0.02	3	
Khairpur	Fall	EL6								**0.29**	0.08	0.03	9	Gall *et al.* (2017)
Khairpur	Fall	EL6								**0.21**	0.02	0.01	11	Klaver *et al.* (2020)
Khairpur Avg.						3.3	–			**0.25**	0.09			
Atlanta	Find	EL6				2.3	–			**0.21**	0.03	0.01	8	Klaver *et al.* (2020)
Hvittis	Fall	EL6				2.4	0.3			**0.22**	0.02	0.01	7	Klaver *et al.* (2020)
Yilmia	Find	EL6								**0.21**	0.02	0.01	8	Klaver *et al.* (2020)
Indarch acid leachates														
magnetic	Fall	EH4								**0.27**	0.03	0.02	2	
non-magnetic sulfides	Fall	EH4								**0.25**	0.07	0.04	3	
non-magnetic sulfides	Fall	EH4								**0.18**	0.04	0.02	4	
non-magnetic silicates	Fall	EH4								**0.27**	0.05	0.04	2	

S content data are from Defouilloy *et al.* (2016). All the bulk enstatite chondrites show average $\delta^{60/58}$Ni values of 0.24 ± 0.08 ‰ (2 s.d., $n = 13$), and the $\delta^{60/58}$Ni variation should not be caused by the S contents.

Table 1 (*Continued*)

Meteorite	Fall/ Find	Type	Petrology	Mass (mg)	Mg#	S content (%)	Uncertainty	Ni content (ppm)	S/Ni	$\delta^{60/58}$Ni (‰)	2 s.d.	2 s.e.	*n*	References, notes
Enstatite achondrites														
Norton County	Fall	Aubrite	Fragmental breccia	~5000	98.1	0.6	0.1	127	86.7	**0.57**	0.06	0.04	2	
Bishopville	Fall	Aubrite	Fragmental breccia	318	97.4	1.0	0.9			**0.34**	0.06	0.04	2	
Bustee	Fall	Aubrite	Regolith breccia	293	97.8	0.1	0.0	50	36.7	**0.14**	0.06	0.04	2	
Larned	Find	Aubrite	Fragmental breccia	500	97.2					**0.13**	0.06	0.04	2	Mostly silicate
Cumberland Falls	Fall	Aubrite	Fragmental breccia	42.01	98.2	1.5	1.0	253	108.8	**0.04**	0.03	0.02	3	
ALH 84007	Find	Aubrite	Fragmental breccia	50.7	99.2			240		**0.21**	0.03	0.02	3	
LAR 04316	Find	Aubrite	Fragmental breccia	76.76	98.6			539		**0.05**	0.03	0.01	4	
Khor Temiki	Fall	Aubrite	Fragmental breccia	69.59	98.8	0.3	–	241	22.8	**0.06**	0.02	0.01	3	
ALHA 78113	Find	Aubrite	Fragmental breccia	72.43	98.3			635		**0.12**	0.01	0.01	3	
Peña Blanca Spring	Fall	Aubrite	Fragmental breccia	~3500	99.4			40		**0.26**	0.01	0.01	4	
Aubres	Fall	Aubrite	Fragmental breccia	307	98.9					**0.18**	0.01	0.01	4	
Pesyanoe	Fall	Aubrite	Regolith breccia	409	98.5					**0.03**	0.03	0.02	3	
Shallow Water	Find	Aubrite	Non-brecciated	30.92	77.7	2.8	–	11485	4.5	**0.18**	0.02	0.01	3	
Itqiy	Find	EH7	Non-brecciated	~50	65.1	0.0	–	13010	0.0	**0.31**	0.01	0.01	4	
Standards														
BHVO-2										**0.03**	0.02	0.01	4	
BHVO-2										**0.04**	0.03	0.02	3	
BCR-1										**0.26**	0.05	0.03	3	
NOD-P										**0.33**	0.06	0.03	4	
Allende	Fall	CV3								**0.35**	0.04	0.02	3	

S content data are from Defouilloy *et al.* (2016). All the bulk enstatite chondrites show average $\delta^{60/58}$Ni values of 0.24 ± 0.08 ‰ (2 s.d., $n = 13$), and the $\delta^{60/58}$Ni variation should not be caused by the S contents.

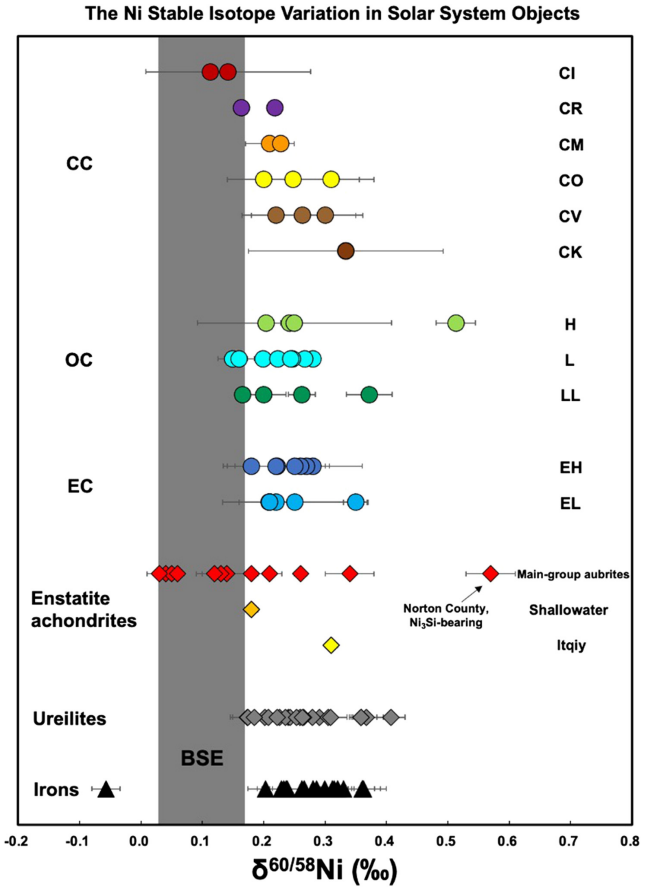

Figure 1 Ni stable isotope composition of solar system materials (Table S-1). Circles and triangles are chondrites and iron meteorites, respectively (Cameron *et al.*, 2009; Steele *et al.*, 2012; Gall *et al.*, 2017; Klaver *et al.*, 2020; Wang *et al.*, 2021), while diamonds are enstatite achondrites and ureilites (Zhu *et al.*, 2022). The uncertainty is mostly at 2 s.e. level, or 2 s.d. level when the 2 s.e. is not available in literature or there are averaged values of multiple data. The grey bar represents the Ni isotope composition of bulk silicate Earth (0.10 ± 0.07 ‰; Klaver *et al.*, 2020; Wang *et al.*, 2021). Enstatite achondrites (diamonds), representing their core composition for Ni, have $\delta^{60/58}$Ni values (0.14 ± 0.18 ‰, 2 s.d.; excluding Norton County) overlapping with ECs, suggesting the core formation does not effectively fractionate Ni isotopes.

chondrites (*i.e.* the potential precursors of enstatite achondrites), is important to understand the Ni isotope fractionation during core formation and the Ni isotope gap between chondrites and BSE (Klaver *et al.*, 2020; Wang *et al.*, 2021; Zhu *et al.*, 2022). Enstatite achondrites are highly reduced (IW−2 to IW−6) like Mercury and rich in sulfide (Mittlefehldt *et al.*, 1998), so their Ni isotope compositions can also be used to constrain the role of metal-sulfide fractionation. On the other hand, the number of Ni isotope data of enstatite chondrites, are limited, and the Ni isotope variation in chondrites is poorly understood. Thus, we determined the Ni stable isotope compositions of both enstatite chondrites (ECs), including the leaching components, and enstatite achondrites for 1) surveying the Ni stable isotope reservoir of ECs, 2) understanding core formation in highly reduced differentiated asteroids, and 3) understanding the possible origin of the Ni stable isotope difference between the Earth and chondrites.

Results

The sample information, elemental and Ni stable isotope data are shown in Table 1. Additional sample information, leaching and analytical methods (using the double spike technique) are provided in detail in the Supplementary Information. Bulk enstatite chondrites show variable $\delta^{60/58}$Ni values ranging from 0.18 ‰ to 0.35 ‰ with an average value of 0.24 ± 0.08 ‰ (2 s.d.) or ± 0.02 ‰ (2 s.e., $n = 13$; Table 1, Fig. 1; including data from the literature). The Ni isotopic variation is independent of the EH or EL grouping, meteorite fall or find and petrological (E3–E6) types. Bulk and leachates (including leachates of the magnetic sulfide-bearing fraction) of magnetically separated phase mixtures of Indarch (EH4) show similar Ni stable isotope compositions (Fig. 2), and no correlation has been found between S contents and $\delta^{60/58}$Ni values for bulk enstatite chondrites (Fig. 3c).

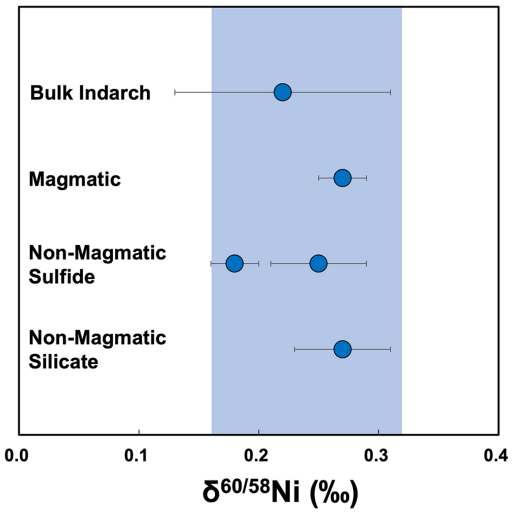

Figure 2 Ni stable isotope compositions of acid leaching phases of Indarch [EH4]. The light blue bar represents the average $\delta^{60/58}$Ni value of bulk ECs. Sulfide phases show similar $\delta^{60/58}$Ni values as bulk and other phases, suggesting the sulfide in chondrites does not cause any Ni isotope variation.

In contrast, Ni stable isotope compositions of enstatite achondrites vary more, ranging from −0.03 ± 0.03 ‰ (Pesyanoe) to 0.57 ± 0.06 ‰ (Norton County). $\delta^{60/58}$Ni values of enstatite achondrites do not correlate with Ni contents nor with Mg#, *i.e.* the molar Mg/(Mg + Fe) ratio (Fig. 3a,b), while their $\delta^{60/58}$Ni values broadly correlate with the S contents and S/Ni ratio (excluding Norton County; Fig. 3c,d). The mean $\delta^{60/58}$Ni values of enstatite achondrites (0.19 ± 0.28 ‰, 2 s.d., $n = 14$) overlap with ECs and BSE. Samples from the three enstatite achondrite parent bodies, *i.e.* main-group aubrites, Shallowater and Itqiy (Zhu *et al.*, 2021) have overlapping Ni isotope compositions.

Discussion

Ni stable isotope composition of enstatite chondrites. No systematic Ni stable isotope variation exists between meteorite falls and finds, suggesting that terrestrial weathering had no, or just a limited, effect on modifying the Ni stable isotope compositions. The $\delta^{60/58}$Ni similarity of Indarch components suggests that Ni stable isotopes may not be fractionated to a measurable degree during nebular and parent body heating processes at this sampling scale, and nor also during the leaching processes (*e.g.*, intermediate leaching phases might adsorb Ni which could induce kinetic isotope fractionation processes). Also considering the lack of correlation between S contents and Ni isotopes for ECs (Fig. 3c), it is difficult to envision that sulfides in chondrites may cause the $\delta^{60/58}$Ni variation in chondrites (Wang *et al.*, 2021;

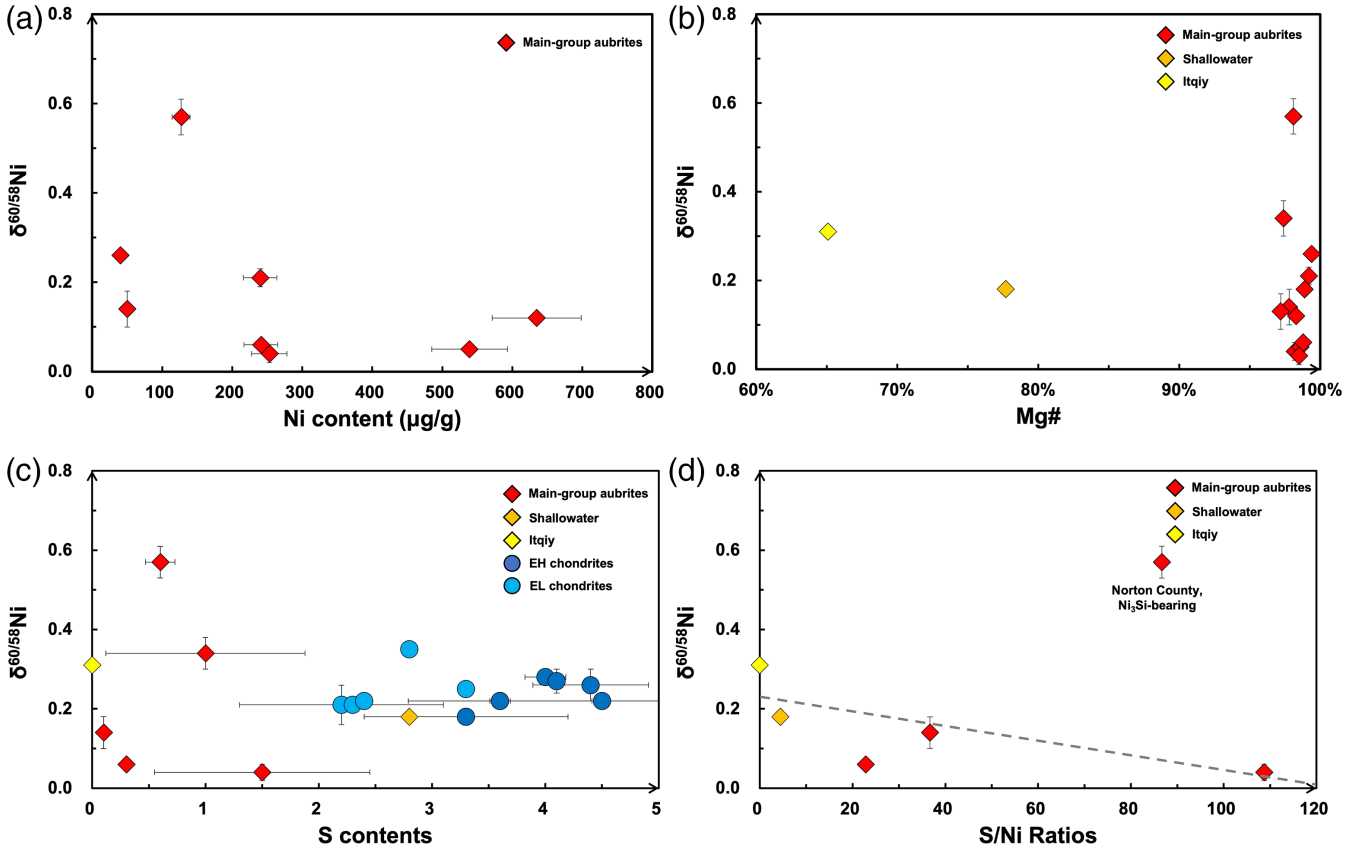

Figure 3 Ni stable isotope compositions *versus* **(a)** Ni contents, **(b)** Mg#, **(c)** sulfur contents and **(d)** S/Ni ratios. The symbols are the same as in Figure 1. EC Ni isotope data are from this study and literature (Cameron *et al.*, 2009; Gall *et al.*, 2017; Klaver *et al.*, 2020; Wang *et al.*, 2021), while S content data are from Defouilloy *et al.* (2016). Lack of correlation between Ni isotopes and Ni contents and Mg# **(a, b)** indicates Ni isotope variation in enstatite achondrites is not caused by silicate differentiation. We also do not find a co-variation between S contents and Ni isotopes in ECs **(c)**, suggesting sulfide does not control the Ni isotope variation in chondrites. A broad correlation between S/Ni ratio and Ni isotopes for enstatite achondrites is consistent with a mixing between sulfide and metal **(d)**.

Fig. 1). Considering that Ca-Al-rich inclusions (CAIs) are extremely rare in ECs and have rather low Ni contents, CAIs are unlikely to contribute to the Ni stable isotope variation in ECs. Some coarse grained CAIs have extremely heavy $\delta^{60/58}$Ni compositions (Render *et al.*, 2018); this implies that the limited $\delta^{60/58}$Ni variation among the ECs, and resolvable but small isotopic variation in other chondrites, could reflect heterogeneities and non-representative sampling of chondrules, matrix and refractory inclusions. Compared to the more equilibrated type 4–6 ECs (with $\delta^{60/58}\text{Ni} = 0.21 \pm 0.04$ ‰, 2 s.d., $n = 6$), the unequilibrated ECs of type 3 possess more variable (larger 2 s.d. uncertainties) $\delta^{60/58}$Ni values (0.28 ± 0.12 ‰, 2 s.d., $n = 6$). This hints that parent body metamorphism equilibrates stable Ni isotopic compositions and thus yields more homogeneous bulk compositions. The average $\delta^{60/58}$Ni composition of ECs is 0.24 ± 0.08 ‰ (2 s.d., $n = 13$), very similar to the mean of ordinary chondrites (OCs; $\delta^{60/58}\text{Ni} = 0.25 \pm 0.18$ ‰, 2 s.d., $n = 16$) and carbonaceous chondrites (CCs; $\delta^{60/58}\text{Ni} = 0.23 \pm 0.12$ ‰, 2 s.d., $n = 13$). This implies a relatively homogeneous $\delta^{60/58}$Ni of 0.24 ± 0.14 ‰ (2 s.d., $n = 43$) of diverse nebular reservoirs and this average composition can be used as a baseline for tracing planetary differentiation, despite the potential for small Ni isotope differences on the typical sampling scale.

Mineralogical control on $\delta^{60/58}$Ni variations in enstatite achondrites. Enstatite achondrites show variable $\delta^{60/58}$Ni values ranging from -0.03 ± 0.03 ‰ to 0.57 ± 0.06 ‰; note, Norton County shows the heaviest $\delta^{60/58}$Ni value among all the enstatite achondrites, which could be caused by the presence of the Ni-rich mineral carletonmooreite (Ni_3Si) (Garvie *et al.*, 2021). The impact of this phase on the Ni isotope composition of bulk Norton County is unknown, however. Lack of correlation between Ni contents and Mg# (Fig. 3b) suggests this variation is not controlled by a simple differentiation and partitioning process involving silicates. This is also consistent in that the enstatite contains little Ni, typically less than the detection limit of electron microprobe analyses (Watters and Prinz, 1979). The Ni budget in enstatite achondrites is dominated by Fe-Ni metal and sulfide (*e.g.*, troilite) with Ni contents of 4–80 wt. % and 0.03–0.9 wt. %, respectively (Casanova *et al.*, 1993; van Acken *et al.*, 2012b). Hence, the $\delta^{60/58}$Ni variation in aubrites may be caused by heterogeneities in the fractions of these minerals, since Ni should have different valance states in metal (Ni^0) and sulfide, phosphides, and other non-metal phases (Ni^{2+}). It is known that magmatic sulfides in terrestrial komatiites can possess isotopically light $\delta^{60/58}$Ni values down to approximately −1 ‰ (Hiebert *et al.*, 2022), however, these rocks formed at very different fO_2 compared to the highly reduced enstatite achondrites. The $\delta^{60/58}$Ni variations in ureilites may also be controlled by isotopically light sulfide, relative to metal (Zhu *et al.*, 2022). In the present data set on enstatite achondrites, a relationship between sulfides and the variation in $\delta^{60/58}$Ni is supported by the correlation between Ni/S ratios and $\delta^{60/58}$Ni (except for Norton County; Fig. 3d). $\delta^{60/58}$Ni variations in enstatite achondrites are both isotopically lighter and heavier compared to chondrites. From these observations we conclude that the variable $\delta^{60/58}$Ni values for the main-group aubrites reflects the mixing of sulfides (light) and metal (heavy) in these

rocks, and the metal-sulfide fractionation factor can also be roughly estimated as $\Delta^{60/58}Ni_{metal\text{-}sulfide} \approx 0.3$ ‰ by the $\delta^{60/58}Ni$ variation amongst enstatite aubrites. This is in accord with the variable $\delta^{60/58}Ni$ values of ureilites and interpretation of metal-sulfide mixing (Zhu *et al.*, 2022). It is also comparable to the $\delta^{60/58}Ni$ variation in iron meteorites (Fig. 3d, Table S-1), which potentially reflect asteroidal core crystallisation (*e.g.*, Ni *et al.*, 2020). Magmatic sulfides in enstatite achondrites have a different petrogenesis compared to sulfides in chondrites which do not show light $\delta^{60/58}Ni$ values. The sulfide minerals in enstatite achondrites are diverse; besides troilite, other Ni-rich minerals may contribute to their bulk Ni isotope compositions, *e.g.*, schreibersite [$(Fe,Ni)_3P$], djerfisherite [$(K,Na)_6(Cu,Fe,Ni)_{25}S_{26}Cl$], lawrencite [$(Fe,Ni)Cl_2$] (Weisberg and Kimura, 2012). In the next section we discuss the origin of the assemblage of Ni-bearing phases in enstatite achondrites and their significance for the difference of $\delta^{60/58}Ni$ between chondrites and the bulk silicate Earth.

$\delta^{60/58}$Ni compositions of enstatite achondrites and core formation of their parent bodies. Since Ni is very abundant in Fe-Ni metal, the measured $\delta^{60/58}Ni$ values of the aubrites (except the acid leaching residue of Larned) should dominantly reflect the composition of the metal in the aubrites. Lack of appreciable fractionation in the trace element signature of the metal suggests that the latter may have been trapped during incomplete metal-silicate segregation in their parent body (Casanova *et al.*, 1993). Van Acken *et al.* (2012b) proposed that the aubrite parent body (ies) experienced a complicated history, including break up and re-accretion by impact, which may have involved trapping of minor metal and sulfide from the cores of their parent bodies. Assuming the metal and sulfide in aubrites represent re-accreted core material, the Ni stable isotope composition of aubrites could be representative of the bulk isotopic composition of the core of the main-group aubrite parent body, *i.e.* $\delta^{60/58}Ni = 0.14 \pm 0.19$ ‰ (2 s.d., $n = 11$; except for Norton County). This large $\delta^{60/58}Ni$ variation of main -group aubrites and large uncertainty of the estimated core $\delta^{60/58}Ni$ composition may reflect heterogeneous sulfide distribution in the core. On the other hand, the acid leaching residue of Larned mostly represents the composition of the silicate portion, and thus the mantle after core formation, of the main-group aubrite parent body. The $\delta^{60/58}Ni$ value of the silicate portion of Larned, 0.13 ± 0.04 ‰ (2 s.e.), could suggest that both the core and mantle of the aubrite parent body have $\delta^{60/58}Ni$ values overlapping those of ECs (0.24 ± 0.08 ‰) and the average of all the chondrites (0.24 ± 0.14 ‰). This suggests limited Ni isotope fraction during the segregation of sulfur-rich cores of the main-group aubrite parent body, *i.e.* S can be present as an FeS phase in the core (*e.g.*, Wood *et al.*, 2014). Shallowater and Itqiy contain more metal and show higher Ni contents relative to main-group aubrites (Keil *et al.*, 1989; Patzer *et al.*, 2001), so their bulk $\delta^{60/58}Ni$ values may also reflect the isotopic composition of the core of their parent bodies. The $\delta^{60/58}Ni$ values, 0.18 ± 0.02 ‰ for Shallowater and 0.31 ± 0.01 ‰ for Itqiy, fall into the average of chondrites too, which is consistent with the conclusion that metal-sulfide segregation processes at highly reduced conditions possibly do not effectively fractionate Ni isotopes. This interpretation of the aubrite data is also supported by the overlapping Ni stable isotope compositions of rocks derived from the mantle of the ureilite parent body and chondrites (Zhu *et al.*, 2022). The mantle of the ureilite parent body also underwent segregation of sulfide melt into its core (Warren *et al.*, 2006). However, this interpretation should be further tested, since 1) metal-sulfide-silicate segregation in aubrite parent bodies may have been incomplete (Casanova *et al.*, 1993), and 2) the $\delta^{60/58}Ni$ variation range for the aubrites is relatively large.

Earth might be built from chondrules, not bulk chondrites. Since core formation cannot be caused by a Ni isotopic gap between chondrites and Earth (Klaver *et al.*, 2020), other possible scenarios include 1) pebble accretion (Zhu *et al.*, 2022), 2) a highly reduced Moon-forming impactor (Wang *et al.*, 2021), and 3) nebular fractionation (Morbidelli *et al.*, 2020). Bulk chondrites are not the only candidates for the precursor material for Earth; instead, chondrules can be the main accretion material for Earth and other terrestrial planets (Johansen *et al.*, 2015), which could be tested by measuring Ni isotope compositions of chondrules, especially chondrules from ECs with Earth-like isotopic signatures (Zhu *et al.*, 2020).

Wang *et al.* (2021) proposed a different model in which the object (Theia) that hit the Earth during the Moon-forming impact was like Mercury, *i.e.* highly reduced, with its mantle rich in sulfur and isotopically light Ni. The Ni isotope data of enstatite achondrites cannot be used to directly test this model because enstatite achondrites are mainly composed of sulfide minerals (Keil, 2010), rather than S^{2-} in silicates (*e.g.*, in the Mercury mantle). This model could be more readily tested by measuring Ni stable isotope compositions of lunar samples and experimental samples of sulfur-rich metal-silicate segregation. Alternatively, this Ni stable isotope fractionation could have occurred during condensation and evaporation at the nebular stage, predating the accretion of the terrestrial planets (Morbidelli *et al.*, 2020).

Acknowledgements

KZ thanks an Alexander von Humboldt postdoc fellowship and a UK STFC grant (no. ST/V000888/1). We thank Jean-Alix Barrat and Fred Moynier for samples. Wei Dai is appreciated for sample preparation. Constructive comments from David van Acken and Paul Savage and editorial handling by Helen Williams are highly appreciated. Discussion from Jing-Ya Hu also improved this manuscript.

Editor: Helen Williams

Additional Information

Supplementary Information accompanies this letter at https://www.geochemicalperspectivesletters.org/article2306.

Cite this letter as: Zhu, K., Becker, H., Zhu, J.-M., Xu, H.-P., Man, Q.-R. (2023) Planetary accretion and core formation inferred from Ni isotopes in enstatite meteorites. *Geochem. Persp. Let.* 25, 1–7. https://doi.org/10.7185/geochemlet.2306

References

Cameron, V., Vance, D., Archer, C., House, C.H. (2009) A biomarker based on the stable isotopes of nickel. *Proceedings of the National Academy of Sciences* 106, 10944–10948. https://doi.org/10.1073/pnas.0900726106

Casanova, I., Keil, K., Newsom, H.E. (1993) Composition of metal in aubrites: Constraints on core formation. *Geochimica et Cosmochimica Acta* 57, 675–682. https://doi.org/10.1016/0016-7037(93)90377-9

Clayton, R.N., Mayeda, T.K., Rubin, A.E. (1984) Oxygen isotopic compositions of enstatite chondrites and aubrites. *Journal of Geophysical Research: Solid Earth* 89, C245–C249. https://doi.org/10.1029/JB089iS01p0C245

Defouilloy, C., Cartigny, P., Assayag, N., Moynier, F., Barrat, J.-A. (2016) High-precision sulfur isotope composition of enstatite meteorites and implications of the formation and evolution of their parent bodies. *Geochimica et Cosmochimica Acta* 172, 393–409. https://doi.org/10.1016/j.gca.2015.10.009

Gall, L., Williams, H.M., Halliday, A.N., Kerr, A.C. (2017) Nickel isotopic composition of the mantle. *Geochimica et Cosmochimica Acta* 199, 196–209. https://doi.org/10.1016/j.gca.2016.11.016

Garvie, L.A.J., Ma, C., Ray, S., Domanik, K., Wittmann, A., Wadhwa, M. (2021) Carletonmooreite, Ni_3Si, a new silicide from the Norton County aubrite meteorite. *American Mineralogist* 106, 1828–1834. https://doi.org/10.2138/am-2021-7645

Guignard, J., Quitté, G., Méheut, M., Toplis, M.J., Poitrasson, F., Connetable, D., Roskosz, M. (2020) Nickel isotope fractionation during metal-silicate differentiation of planetesimals: Experimental petrology and *ab initio* calculations. *Geochimica et Cosmochimica Acta* 269, 238–256. https://doi.org/10.1016/j.gca.2019.10.028

Hiebert, R.S., Bekker, A., Houlé, M.G., Rouxel, O.J. (2022) Nickel isotope fractionation in komatiites and associated sulfides in the hart deposit, Late Archean Abitibi Greenstone Belt, Canada. *Chemical Geology* 603, 120912. https://doi.org/10.1016/j.chemgeo.2022.120912

Johansen, A., Low, M.-M.M., Lacerda, P., Bizzarro, M. (2015) Growth of asteroids, planetary embryos, and Kuiper belt objects by chondrule accretion. *Science Advances* 1, e1500109. https://doi.org/10.1126/sciadv.1500109

Keil, K. (2010) Enstatite achondrite meteorites (aubrites) and the histories of their asteroidal parent bodies. *Geochemistry* 70, 295–317. https://doi.org/10.1016/j.chemer.2010.02.002

Keil, K., Ntaflos, T., Taylor, G.J., Brearley, A.J., Newsom, H.E., Romig Jr., A.D. (1989) The Shallowater aubrite: Evidence for origin by planetesimal impacts. *Geochimica et Cosmochimica Acta* 53, 3291–3307. https://doi.org/10.1016/0016-7037(89)90108-7

Klaver, M., Ionov, D.A., Takazawa, E., Elliott, T. (2020) The non-chondritic Ni isotope composition of Earth's mantle. *Geochimica et Cosmochimica Acta* 268, 405–421. https://doi.org/10.1016/j.gca.2019.10.017

Lazar, C., Young, E.D., Manning, C.E. (2012) Experimental determination of equilibrium nickel isotope fractionation between metal and silicate from 500 °C to 950 °C. *Geochimica et Cosmochimica Acta* 86, 276–295. https://doi.org/10.1016/j.gca.2012.02.024

Mittlefehldt, D.W., McCoy, T.J., Goodrich, C.A., Kracher, A. (1998) Non-chondritic meteorites from asteroidal bodies. In: Papike, J.J. (Ed.) *Reviews in Mineralogy 36: Planetary Materials*. De Gruyter, Berlin, 1–195. https://doi.org/10.1515/9781501508806-019

Morbidelli, A., Libourel, G., Palme, H., Jacobson, S.A., Rubie, D.C. (2020) Subsolar Al/Si and Mg/Si ratios of non-carbonaceous chondrites reveal planetesimal formation during early condensation in the protoplanetary disk. *Earth and Planetary Science Letters* 538, 116220. https://doi.org/10.1016/j.epsl.2020.116220

Ni, P., Chabot, N.L., Ryan, C.J., Shahar, A. (2020) Heavy iron isotope composition of iron meteorites explained by core crystallization. *Nature Geoscience* 13, 611–615. https://doi.org/10.1038/s41561-020-0617-y

Patzer, A., Hill, D.H., Boynton, W.V. (2001) Itqiy: A metal-rich enstatite meteorite with achondritic texture. *Meteoritics and Planetary Science* 36, 1495–1505. https://doi.org/10.1111/j.1945-5100.2001.tb01841.x

Render, J., Brennecka, G.A., Wang, S.-J., Wasylenki, L.E., Kleine, T. (2018) A Distinct Nucleosynthetic Heritage for Early Solar System Solids Recorded by Ni Isotope Signatures. *The Astrophysical Journal* 862, 26. https://doi.org/10.3847/1538-4357/aacb7e

Steele, R.C.J., Coath, C.D., Regelous, M., Russell, S., Elliott, T. (2012) Neutron-poor nickel isotope anomalies in meteorites. *The Astrophysical Journal* 758, 59. https://doi.org/10.1088/0004-637X/758/1/59

van Acken, D., Brandon, A.D., Lapen, T.J. (2012a) Highly siderophile element and osmium isotope evidence for postcore formation magmatic and impact processes on the aubrite parent body. *Meteoritics and Planetary Science* 47, 1606–1623. https://doi.org/10.1111/j.1945-5100.2012.01425.x

van Acken, D., Humayun, M., Brandon, A.D., Peslier, A.H. (2012b) Siderophile trace elements in metals and sulfides in enstatite achondrites record planetary differentiation in an enstatite chondritic parent body. *Geochimica et Cosmochimica Acta* 83, 272–291. https://doi.org/10.1016/j.gca.2011.12.025

Wang, S.-J., Wang, W., Zhu, J.-M., Wu, Z., Liu, J., Han, G., Teng, F.-Z., Huang, S., Wu, H., Wang, Y., Wu, G., Li, W. (2021) Nickel isotopic evidence for late-stage accretion of Mercury-like differentiated planetary embryos. *Nature Communications* 12, 294. https://doi.org/10.1038/s41467-020-20525-1

Warren, P.H., Ulff-Møller, F., Huber, H., Kallemeyn, G.W. (2006) Siderophile geochemistry of ureilites: A record of early stages of planetesimal core formation. *Geochimica et Cosmochimica Acta* 70, 2104–2126. https://doi.org/10.1016/j.gca.2005.12.026

Watters, T.R., Prinz, M. (1979) Aubrites: Their origin and relationship to enstatite chondrites. *Proceedings of the 10th Lunar and Planetary Science Conference*, 19–23 March 1979, Houston, Texas, 1073–1093. https://articles.adsabs.harvard.edu/pdf/1979LPSC…10.1073W

Weisberg, M.K., Kimura, M. (2012) The unequilibrated enstatite chondrites. *Geochemistry* 72, 101–115. https://doi.org/10.1016/j.chemer.2012.04.003

Wood, B.J., Kiseeva, E.S., Mirolo, F.J. (2014) Accretion and core formation: The effects of sulfur on metal–silicate partition coefficients. *Geochimica et Cosmochimica Acta* 145, 248–267. https://doi.org/10.1016/j.gca.2014.09.002

Wood, B.J., Smythe, D.J., Harrison, T. (2019) The condensation temperatures of the elements: A reappraisal. *American Mineralogist* 104, 844–856. https://doi.org/10.2138/am-2019-6852CCBY

Zhu, K., Moynier, F., Schiller, M., Bizzarro, M. (2020) Dating and Tracing the Origin of Enstatite Chondrite Chondrules with Cr Isotopes. *The Astrophysical Journal Letters* 894, L26. https://doi.org/10.3847/2041-8213/ab8dca

Zhu, K., Moynier, F., Schiller, M., Becker, H., Barrat, J.A., Bizzarro, M. (2021) Tracing the origin and core formation of the enstatite achondrite parent bodies using Cr isotopes. *Geochimica et Cosmochimica Acta* 308, 256–272. https://doi.org/10.1016/j.gca.2021.05.053

Zhu, K., Barrat, J.-A., Yamaguchi, A., Rouxel, O., Germain, Y., Langlade, J., Moynier, F. (2022) Nickel and Chromium Stable Isotopic Composition of Ureilites: Implications for the Earth's Core Formation and Differentiation of the Ureilite Parent Body. *Geophysical Research Letters* 49, e2021GL095557. https://doi.org/10.1029/2021GL095557

Geochemical Perspectives Letters

Planetary accretion and core formation inferred from Ni isotopes in enstatite meteorites

K. Zhu, H. Becker, J.-M. Zhu, H.-P. Xu, Q.-R. Man

Supplementary Information

The Supplementary Information includes:

- Samples and Analytical Methods
- Table S-1
- Supplementary Information References

Samples and Analytical Methods

The enstatite chondrites, including MAC 88184 [EL3], MAC 02837 [EL3], GRO 95517 [EH3], Qingzhen [EH3], SAH 97096 [EH3] and Indarch [EH4], Itqiy [EH7] and the acid leachates of Indarch are from the dissolution in Zhu *et al.* (2021a). Bulk chondrite samples were dissolved in Teflon bombs + Evapo Clean at 140 °C using concentrated HF + HNO_3 (2:1) for 2 days and concentrated aqua regia (HCl + HNO_3, 3:1) at 140 °C for another 2 days following a protocol described in Inglis *et al.* (2018).

We performed the acid leaching for Indarch and tried to obtain its different phases. The sample solutions are from Zhu *et al.* (2021a), and related method is following Moynier *et al.* (2011). the magnetic fractions (from sample powders) were collected using a hand magnet and dissolved in aqua regia in Teflon bombs at 140 °C for 2 days. Note that the magnetic fractions were not pure metal and included other Fe-Ni-bearing minerals, such as troilite that can be also separated by magnet. After extraction of the magnetic fraction, the residual nonmagnetic fraction (mostly silicates and other sulfide) was then dissolved in cold 3 N HCl for ~6 hr to dissolve the sulfides. Since some Fe-Ni-bearing sulfide has been extracted in last step, only some Fe-Ni-poor sulfide was dissolved in this procedure. The final residues (mostly silicates) were dissolved in concentrated HF + HNO_3 at 140 °C for 2 days and concentrated aqua regia at 140 °C for another 2 days in Teflon bombs to completely dissolve the silicates.

We selected 14 enstatite achondrites for Ni isotope measurements in this study (Table 1). Twelve of them are main-group aubrites, with one anomalous aubrite Shallowater and another enstatite-rich EH7 meteorite, Itqiy. Note that, the three groups of enstatite meteorites can represent three different parent bodies based on their mass-independent $^{54}Cr/^{52}Cr$ compositions (Zhu *et al.*, 2021b). The petrological description for main-group aubrites and Shallowater can be found in Keil (2010), and that for Itqiy is introduced in (Patzer *et al.*, 2001). Except Shallowater and Itqiy, all the main-group aubrites in this study are breccia meteorites (Keil, 2010). Some of the aubrites, including Norton County, Bishopville, Bustee, Larned, Peña Blanca Spring, Aubres and Pesyanoe, are from the dissolution in Barrat *et al.* (2016). These meteorite samples were firstly powdered using a boron carbide mortar and pestle, and then the powers were dissolved in closed screw-top teflon vessels (Savillex) at about 130 °C for three days using 5 mL of concentrated HF, and 2 mL of concentrated HNO_3. The vessels were then opened. After evaporation to dryness of the acid mixture, approximately 2 mL of HNO_3 was added, and the vessels were capped and placed back on the hot plate and left overnight. Note that, Larned (sample powder) was leached in hot 6 N HCl (1 h, 120 °C), to dissolve all

sulfides (including troilite) and the Fe-Ni metal, leaving residues composed essentially of silicate phases (mainly enstatite and sometimes diopside and plagioclase). Cumberland Falls, ALH 84007 and Shallowater are from the dissolution in Zhu *et al.* (2021b) that is the same as the protocol for the bulk enstatite chondrites in this study. The remaining aubrites, LAR 04316, Khor Temiki, ALHA 78113, were weighed and dissolved in Parr Bombs at Freie Universität Berlin. The samples were dissolved in a mixing acid of 3 mL conc. HF and 1 mL conc. HNO_3 at 180 °C for two days. After drying down, the samples were redissolved in 3 mL conc. HNO_3 at 180 °C for another two days; then no visible particles were observed in the sample dissolutions.

For all sample solutions, Before the addition of a ^{61}Ni-^{62}Ni double spike, 1 % of the sample solutions were analysed for element mass fractions on a Thermo Instrument Element II Inductively Coupled Plasma Mass Spectrometer, housed at China University of Geosciences (Beijing). For stable isotope compositions, 400–800 ng of Ni were mixed with the double spike. The sample and spikes were heated in 6 N HCl in Teflon beaker at 120 °C over night for complete homogenisation. We employed a five-step column chemistry to purify the sample solutions, and the related method is described in Wu *et al.* (2019, 2022). The Ni yields of the entire purification procedure were >90 %, and the total Ni blanks were <1.2 ng, consistent with our previous work. After the column chemistry, conc. HNO_3 (0.6 mL) + 30 % H_2O_2 (0.3 mL) were added to the samples and heated at 130 °C overnight, for destroying any organics that may have potentially leached from the resin.

The Ni stable isotope measurements were performed on a Neptune Plus Multicollector-Inductively Coupled Plasma Mass Spectrometer housed at China University of Geosciences (Beijing). The methods are the same as those used in Wu *et al.* (2019, 2022). The instrument is equipped with nine Faraday Cups, and each cup are connected to a 1011 X amplifier. The signal intensities of ^{57}Fe, ^{58}Ni + ^{58}Fe, ^{60}Ni, ^{61}Ni, ^{62}Ni and ^{64}Ni were simultaneously measured using L3, L2, C, H1, H2 and H4 cups in static mode, respectively. We use standard sample + skimmer X cones for a high sensitivity measurement, which also includes an Aridus II desolvator equipped with an ice chamber (Wu *et al.*, 2020) and a 110 µL min^{-1} microconcentric PFA nebuliser (ESI). All the Ni isotope measurements are run in a low-resolution mode and at peak centre. The measurements yielded a ^{60}Ni (centre cup) signal of 10–15 V for both samples and standard solutions. Each measurement consisted of 45 cycles, with an integration time of 4.194 s for each cycle. Blank measurements with 15 cycles of 4.194 s were done and subtracted from the signals of sample solutions (off-line). Other instrumental parameters can be found in detail in (Li *et al.*, 2020). The data precision in study (2 s.d. uncertainty of ~0.02–0.06) are comparable to those in literature (Cameron *et al.*, 2009; Gall *et al.*, 2017; Klaver *et al.*, 2020; Saunders *et al.*, 2020, 2022; Wang *et al.*, 2021). All the measurements in this study were run in two sessions.

We also report the $\delta^{60/58}$Ni data for USGS reference materials, BHVO-2, BCR-1 and NOD-P, and these data consistent with literature data (Cameron *et al.*, 2009; Chernonozhkin *et al.*, 2016; Gall *et al.*, 2017; Klaver *et al.*, 2020; Saunders *et al.*, 2020; Wang *et al.*, 2021) and confirms the high-quality of our data. However, the $\delta^{60/58}$Ni datum for Allende (CV3; see Table S-1) does not overlap with the literature data (Gall *et al.*, 2017; Klaver *et al.*, 2020; Wang *et al.*, 2021), which may reflect sample heterogeneity. Similar inconsistencies were also found in other chondrites, *e.g.*, Orgueil [CI1], Karoonda [CK4] and Barratta [L4] (Gall *et al.*, 2017; Klaver *et al.*, 2020; Wang *et al.*, 2021).

Supplementary Table

Table S-1 Ni stable isotope compositions of chondrites and iron meteorites.

Sample	Group	$\delta^{60/58}$Ni (‰)	2 s.d.	2 s.e.	*n*	References
CCs						
Orgueil	CI1	**0.21**	0.07			Cameron *et al*. (2009)
Orgueil	CI1	**0.19**		0.02		Steele *et al*. (2012)
Orgueil	CI1	**0.18**	0.04	0.02	4	Gall *et al*. (2017)
Orgueil	CI1	**0.02**	0.02	0.01	8	Klaver *et al*. (2020)
Orgueil	CI1	**0.12**	0.02	0.01	8	Klaver *et al*. (2020)
Orgueil	CI1	**0.14**	0.05	0.02	4	Zhu *et al*. (2022)
Orgueil Avg.		**0.14**	0.13			
Ivuna	CI1	**0.11**	0.02	0.01	8	Klaver *et al*. (2020)
Murchison	CM2	**0.21**	0.03			Cameron *et al*. (2009)
Murchison	CM2	**0.23**	0.07	0.04	9	Gall *et al*. (2017)
Murchison	CM2	**0.19**	0.03	0.01	8	Klaver *et al*. (2020)
Murchison Avg.		**0.21**	0.04			
Paris	CM2	**0.23**	0.02		4	Zhu *et al*. (2022)
Kainsaz	CO3.2	**0.20**	0.03	0.01	8	Klaver *et al*. (2020)
Felix	CO3.3	**0.31**	0.07			Cameron *et al*. (2009)
Ornans	CO3.4	**0.29**	0.08	0.03	9	Gall *et al*. (2017)
Ornans	CO3.4	**0.21**	0.02	0.01	8	Klaver *et al*. (2020)
Ornans Avg.		**0.25**	0.11			
Renazzo	CR2	**0.16**	0.03	0.01	8	Klaver *et al*. (2020)
Al Rais	CR2	**0.22**	0.02	0.01	8	Klaver *et al*. (2020)
Leoville	CV3.1	**0.30**	0.05			Cameron *et al*. (2009)
Kaba	CV3.1	**0.22**	0.04			Wang *et al*. (2021)
Allende	CV3.6	**0.24**	0.07	0.02	9	Gall *et al*. (2017)
Allende	CV3.6	**0.24**	0.03	0.01	8	Klaver *et al*. (2020)
Allende	CV3.6	**0.25**	0.04			Wang *et al*. (2021)
Allende	CV3.6	**0.23**	0.02	0.01	4	Zhu *et al*. (2022)
Allende	CV3.6	**0.35**	0.04			This study
Allende Avg.		**0.26**	0.10			
Karoonda	CK4	**0.28**	0.02	0.01	8	Klaver *et al*. (2020)
Karoonda	CK4	**0.39**	0.04			Wang *et al*. (2021)
Karoonda Avg.		**0.33**	0.16			
ECs						
GRO 95517	EH3	**0.28**	0.03	0.02	2	This study
Qingzhen	EH3	**0.27**	0.04	0.03	2	This study
SAH 97096	EH3	**0.26**	0.06	0.04	2	This study
Kota-kota	EH3	**0.20**	0.03	0.01	8	Klaver *et al*. (2020)
Kota-kota	EH3	**0.26**	0.04			Wang *et al*. (2021)
Kota-kota	EH3	**0.21**	0.04			Wang *et al*. (2021)
Kota-kota Avg.		**0.22**	0.07			
Abee	EH4	**0.19**	0.05			Cameron *et al*. (2009)
Abee	EH4	**0.25**	0.02	0.01	7	Klaver *et al*. (2020)
Abee Avg.		**0.22**	0.09			
Indarch	EH4	**0.27**	0.09	0.03	9	Gall *et al*. (2017)
Indarch	EH4	**0.29**	0.05	0.04	2	This study
Indarch	EH4	**0.19**	0.03	0.01	8	Klaver *et al*. (2020)
Indarch Avg.		**0.25**	0.11			

Table S-1 continued.

Sample	Group	$\delta^{60/58}$Ni (‰)	2 s.d.	2 s.e.	*n*	References
ECs (continued)						
St. Mark's	EH5	**0.18**	0.02	0.01	15	Klaver *et al*. (2020)
MAC 88184	EL3	**0.21**	0.08	0.05	2	This study
MAC 02837	EL3	**0.35**	0.03	0.02	3	This study
Khairpur	EL6	**0.29**	0.08	0.03	9	Gall *et al*. (2017)
Khairpur	EL6	**0.21**	0.02	0.01	11	Klaver *et al*. (2020)
Khairpur Avg.		**0.25**	0.12			
Atlanta	EL6	**0.21**	0.03	0.01	8	Klaver *et al*. (2020)
Hvittis	EL6	**0.22**	0.02	0.01	7	Klaver *et al*. (2020)
Yilmia	EL6	**0.21**	0.02	0.01	8	Klaver *et al*. (2020)
OCs						
A 10224	L3	**0.24**	0.01		3–5	Chernonozhkin *et al*. (2016)
Ceniceros	L3.7	**0.20**	0.03	0.01	8	Klaver *et al*. (2020)
Barratta	L4	**0.31**	0.05	0.02	9	Gall *et al*. (2017)
Barratta	L4	**0.19**	0.03	0.01	8	Klaver *et al*. (2020)
Barratta Avg.		**0.25**	0.16			
Bruderheim	L6	**0.51**	0.07	0.03	5	Gall *et al*. (2017)
Chainpur	LL3.4	**0.28**	0.10			Cameron *et al*. (2009)
Chainpur	LL3.4	**0.28**	0.04			Wang *et al*. (2021)
Chainpur Avg.		**0.28**	0.00			
Parnalee	LL3.6	**0.20**	0.03	0.01	8	Klaver *et al*. (2020)
A 09135	LL3	**0.15**	0.02		3–5	Chernonozhkin *et al*. (2016)
Parnalee	LL3	**0.16**	0.05	0.02	4	Gall *et al*. (2017)
Chelyabinsk	LL5	**0.27**	0.03	0.01	8	Klaver *et al*. (2020)
Dhurmsala	LL6	**0.22**	0.02	0.01	8	Klaver *et al*. (2020)
Kilabo	LL6	**0.25**	0.03	0.01	8	Klaver *et al*. (2020)
St. Severin	LL6	**0.24**	0.05		5	Gall *et al*. (2017)
A 09436	H3	**0.20**	0.04		3–5	Chernonozhkin *et al*. (2016)
Bremervorde	H3	**0.26**	0.05	0.03	5	Gall *et al*. (2017)
Buzzard Coulee	H4	**0.17**	0.03	0.01	8	Klaver *et al*. (2020)
Kernouve	H6	**0.37**	0.08	0.04	4	Gall *et al*. (2017)
Irons						
Negrillos	IIA	**0.31**	0.03	0.01	6	Gall *et al*. (2017)
North Chile	IIA	**0.36**	0.05	0.02	6	Gall *et al*. (2017)
Arispe	IC	**0.20**	0.06	0.03	5	Gall *et al*. (2017)
Clark County	IIIF	**0.30**	0.05	0.02	6	Gall *et al*. (2017)
Duel Hill	IVA	**−0.06**	0.06	0.02	6	Gall *et al*. (2017)
Gibeon	IVA	**0.31**	0.06	0.03	6	Gall *et al*. (2017)
Sikhote Alin	IIAB	**0.30**	0.06	0.03	6	Gall *et al*. (2017)
Charcas	IIIA	**0.23**	0.07	0.03	6	Gall *et al*. (2017)
Henbury	IIIA	**0.29**	0.07	0.03	6	Gall *et al*. (2017)
Coahuila	IIAB	**0.36**		0.04		Cameron *et al*. (2009)
Henbury	IIIAB	**0.24**		0.07		Cameron *et al*. (2009)
Bristol	IVA	**0.28**		0.05		Cameron *et al*. (2009)
Hoba	IVB	**0.33**		0.06		Cameron *et al*. (2009)
Santa Clara	IVB	**0.32**		0.03		Steele *et al*. (2011)
Nantan	IICD	**0.32**	0.03	0.02	3	Gueguen *et al*. (2013)
Gibeon	IVA	**0.26**	0.05	0.03	3	Gueguen *et al*. (2013)
Sikhote Alin	IIAB	**0.23**	0.10		3–5	Chernonozhkin *et al*. (2016)
Chinga	IVAB	**0.24**	0.03		3–5	Chernonozhkin *et al*. (2016)
Elga	IIE	**0.24**	0.04		3–5	Chernonozhkin *et al*. (2016)
Darinskoe	IIC	**0.23**	0.04		3–5	Chernonozhkin *et al*. (2016)

Supplementary Information References

Barrat, J.A., Greenwood, R.C., Keil, K., Rouget, M.L., Boesenberg, J.S., Zanda, B., Franchi, I.A. (2016) The origin of aubrites: Evidence from lithophile trace element abundances and oxygen isotope compositions. *Geochimica et Cosmochimica Acta* 192, 29–48. https://doi.org/10.1016/j.gca.2016.07.025

Cameron, V., Vance, D., Archer, C., House, C.H. (2009) A biomarker based on the stable isotopes of nickel. *Proceedings of the National Academy of Sciences* 106, 10944–10948. https://doi.org/10.1073/pnas.0900726106

Chernonozhkin, S.M., Goderis, S., Costas-Rodríguez, M., Claeys, P., Vanhaecke, F. (2016) Effect of parent body evolution on equilibrium and kinetic isotope fractionation: a combined Ni and Fe isotope study of iron and stony-iron meteorites. *Geochimica et Cosmochimica Acta* 186, 168–188. https://doi.org/10.1016/j.gca.2016.04.050

Gall, L., Williams, H.M., Halliday, A.N., Kerr, A.C. (2017) Nickel isotopic composition of the mantle. *Geochimica et Cosmochimica Acta* 199, 196–209. https://doi.org/10.1016/j.gca.2016.11.016

Gueguen, B., Rouxel, O., Ponzevera, E., Bekker, A., Fouquet, Y. (2013) Nickel Isotope Variations in Terrestrial Silicate Rocks and Geological Reference Materials Measured by MC-ICP-MS. *Geostandards and Geoanalytical Research* 37, 297–317. https://doi.org/10.1111/j.1751-908X.2013.00209.x

Inglis, E.C., Creech, J.B., Deng, Z., Moynier, F. (2018) High-precision zirconium stable isotope measurements of geological reference materials as measured by double-spike MC-ICPMS. *Chemical Geology* 493, 544–552. https://doi.org/10.1016/j.chemgeo.2018.07.007

Keil, K. (2010) Enstatite achondrite meteorites (aubrites) and the histories of their asteroidal parent bodies. *Geochemistry* 70, 295–317. https://doi.org/10.1016/j.chemer.2010.02.002

Klaver, M., Ionov, D.A., Takazawa, E., Elliott, T. (2020) The non-chondritic Ni isotope composition of Earth's mantle. *Geochimica et Cosmochimica Acta* 268, 405–421. https://doi.org/10.1016/j.gca.2019.10.017

Li, W., Zhu, J.-M., Tan, D., Han, G., Zhao, Z., Wu, G. (2020) The $\delta^{60/58}$Ni Values of Twenty-Six Selected Geological Reference Materials. *Geostandards and Geoanalytical Research* 44, 523–535. https://doi.org/10.1111/ggr.12321

Moynier, F., Paniello, R.C., Gounelle, M., Albarède, F., Beck, P., Podosek, F., Zanda, B. (2011) Nature of volatile depletion and genetic relationships in enstatite chondrites and aubrites inferred from Zn isotopes. *Geochimica et Cosmochimica Acta* 75, 297–307. https://doi.org/10.1016/j.gca.2010.09.022

Patzer, A., Hill, D.H., Boynton, W.V. (2001) Itqiy: A metal-rich enstatite meteorite with achondritic texture. *Meteoritics and Planetary Science* 36, 1495–1505. https://doi.org/10.1111/j.1945-5100.2001.tb01841.x

Saunders, N.J., Barling, J., Harvey, J., Halliday, A.N. (2020) Heterogeneous nickel isotopic compositions in the terrestrial mantle – Part 1: Ultramafic lithologies. *Geochimica et Cosmochimica Acta* 285, 129–149. https://doi.org/10.1016/j.gca.2020.06.029

Saunders, N.J., Barling, J., Harvey, J., Fitton, J.G., Halliday, A.N. (2022) Heterogeneous nickel isotope compositions of the terrestrial mantle – Part 2: Mafic lithologies. *Geochimica et Cosmochimica Acta* 317, 349–364. https://doi.org/10.1016/j.gca.2021.11.011

Steele, R.C.J., Elliott, T., Coath, C.D., Regelous, M. (2011) Confirmation of mass-independent Ni isotopic variability in iron meteorites. *Geochimica et Cosmochimica Acta* 75, 7906–7925. https://doi.org/10.1016/j.gca.2011.08.030

Steele, R.C.J., Coath, C.D., Regelous, M., Russell, S., Elliott, T. (2012) Neutron-poor nickel isotope anomalies in meteorites. *The Astrophysical Journal* 758, 59. https://doi.org/10.1088/0004-637X/758/1/59

Wang, S.-J., Wang, W., Zhu, J.-M., Wu, Z., Liu, J., Han, G., Teng, F.-Z., Huang, S., Wu, H., Wang, Y., Wu, G., Li, W. (2021) Nickel isotopic evidence for late-stage accretion of Mercury-like differentiated planetary embryos. *Nature Communications* 12, 294. https://doi.org/10.1038/s41467-020-20525-1

Wu, G., Zhu, J.-M., Wang, X., Han, G., Tan, D., Wang, S.-J. (2019) A novel purification method for high precision measurement of Ni isotopes by double spike MC-ICP-MS. *Journal of Analytical Atomic Spectrometry* 34, 1639–1651. https://doi.org/10.1039/C9JA00077A

Wu, G., Zhu, J.-M., Wang, X., Johnson, T.M., Han, G. (2020) High-Sensitivity Measurement of Cr Isotopes by Double Spike MC-ICP-MS at the 10 ng Level. *Analytical Chemistry* 92, 1463–1469. https://doi.org/10.1021/acs.analchem.9b04704

Wu, G., Zhu, J.-M., Wang, X., Johnson, T.M., He, Y., Huang, F., Wang, L.-X., Lai, S.-C. (2022) Nickel isotopic composition of the upper continental crust. *Geochimica et Cosmochimica Acta* 332, 263–284. https://doi.org/10.1016/j.gca.2022.06.019

Zhu, K., Moynier, F., Alexander, C.M.O'D., Davidson, J., Schrader, D.L., Zhu, J.-M., Wu, G.-L., Schiller, M., Bizzarro, M., Becker, H. (2021a) Chromium Stable Isotope Panorama of Chondrites and Implications for Earth Early Accretion. *The Astrophysical Journal* 923, 94. https://doi.org/10.3847/1538-4357/ac2570

Zhu, K., Moynier, F., Schiller, M., Becker, H., Barrat, J.-A., Bizzarro, M. (2021b) Tracing the origin and core formation of the enstatite achondrite parent bodies using Cr isotopes. *Geochimica et Cosmochimica Acta* 308, 256–272. https://doi.org/10.1016/j.gca.2021.05.053

Zhu, K., Barrat, J.-A., Yamaguchi, A., Rouxel, O., Germain, Y., Langlade, J., Moynier, F. (2022) Nickel and Chromium Stable Isotopic Composition of Ureilites: Implications for the Earth's Core Formation and Differentiation of the Ureilite Parent Body. *Geophysical Research Letters* 49, e2021GL095557. https://doi.org/10.1029/2021GL095557